JOURNAL OF GEOPHYSICAL RESEARCH, VOL. 106, NO. A7, 13215–13218, DOI:10.1029/2001JA900026, 2001

# Nonlinear competition between the whistler and Alfvén fire hoses

P. Hellinger

Institute of Atmospheric Physics, Prague, Czech Republic

H. Matsumoto

Radio Science Center for Space & Atmosphere, Kyoto University, Uji, Japan

**Abstract.** We examine a competition between the whistler and Alfvén fire hoses driven by bi-Maxwellian protons with $T_{p\|} > T_{p\perp}$, where $T_{p\|}$ and $T_{p\perp}$ are proton temperatures, parallel and perpendicular to the background magnetic field, respectively. We extend the work of *Hellinger and Matsumoto* [2000] using a two-dimensional hybrid simulation that includes both the instabilities. In the simulation the whistler fire hose initially dominates and saturates in a quasi-linear manner. The Alfvén fire hose is not strongly affected by the presence of the whistler fire hose and grows even when the former is saturated. However, as the Alfvén fire hose grows and saturates via a conversion to Alfvén waves that heat the protons, the waves driven by the whistler fire hose get strongly damped and disappear. The Alfvén waves damp as well, so that at the end of the simulation the wave activity is low. The strong decay of the generated waves translates to an important decrease of the proton temperature anisotropy.

## 1. Introduction

An excess of free energy drives often two different instabilities. The competition process between the two instabilities depends strongly on their linear growth rates but also on their properties (saturation mechanisms) and on the initial wave amplitudes [cf. *Hellinger and Mangeney*, 1999]. In this paper we study the nonlinear competition between the whistler [*Quest and Shapiro*, 1996; *Gary et al.*, 1998] and Alfvén fire hoses [*Hellinger and Matsumoto*, 2000] driven by anisotropic protons with $T_{p\|} > T_{p\perp}$, where $T_{p\|}$ and $T_{p\perp}$ are proton temperatures, parallel and perpendicular to the background magnetic field, respectively. *Hellinger and Matsumoto* [2000] (referred to hereinafter as paper 1) studied the properties of the two instabilities using a linear dispersion solver and one-dimensional (1-D) hybrid simulations. *Gary et al.* [1998] (compare paper 1) have shown that the whistler fire hose has essentially a quasi-linear evolution. On the other hand, paper 1 has revealed that the Alfvén fire hose presents a complicated behavior: For sake of illustration and later reference we present the results of the 1-D simulations of paper 1 in Figure 1. Figure 1 displays the time evolution (time given in units of inverse proton gyrofrequency) of proton anisotropy $T_{p\perp}/T_{p\|}$ (left panel) and energy in fluctuating magnetic field (right panel) for the two instabilities: the whistler fire hose and the Alfvén fire hose. Figure 1 shows clearly the quasi-linear evolution of the whistler fire hose. On the other hand, the Alfvén fire hose displays a clearly non-quasi-linear evolution; detailed analysis of paper 1 shows that during its evolution the initially unstable mode is transitory and converts to strongly damped Alfvén waves. As a consequence, the Alfvén fire hose is very efficient at destroying the proton anisotropy. The 1-D simulation study of paper 1 was very useful for studying the properties of the two instabilities, but in reality the two instabilities coexist and compete. In the present paper we address the question of the competition between the two instabilities using a two-dimensional (2-D) hybrid code simulation that includes both the physical processes. The paper is organized as follows: Section 2 describes the code and the simulation results; section 3 contains a discussion of the results and a conclusion.


0148-0227/05/2001JA900026$9.00

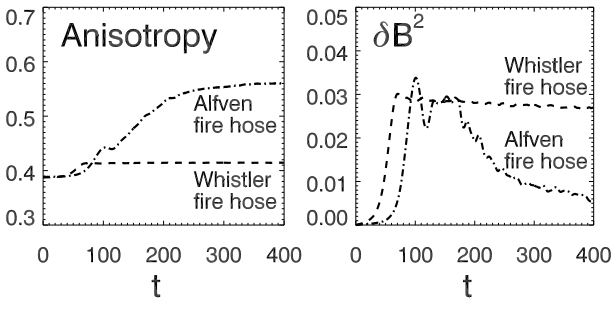


**Figure 1.** Evolution of (left) the temperature anisotropy $T_\perp/T_\|$ and (right) the total fluctuating magnetic energy $\delta B^2$. Evolution is shown for whistler (dashed curve) and Alfvén (dash-dotted curve) fire hoses observed in the one-dimensional simulations of paper 1.

## 2. Simulations

### 2.1. Code

For the numerical simulation we use a 2-D hybrid code developed by *Matthews* [1994]. In this code, electrons are considered as a massless fluid, with a constant temperature; ions are treated as particles and are advanced by a leapfrog scheme that requires the fields to be known at half time steps ahead of the particle velocities. This is obtained by advancing the current density to this time step with only one computational pass through the particle data at each time step. The particle contribution to the current density at the relevant nodes is evaluated with bilinear weighting followed by smoothing over three points. No smoothing is performed on the electromagnetic fields, and the resistivity is set to zero in Ohm's law. The magnetic field is advanced in time with a modified midpoint method, which allows time substepping for the advance of the field.

The units and parameters of the simulation are the following: Units of space and time are $c/\omega_{pi}$ and $\Omega_i$, respectively, where $\omega_{pi} = (n_p e^2/m_p\epsilon_0)^{1/2}$ is the proton plasma frequency and $\Omega_i = eB_0/m_p$ is the proton gyrofrequency. In these expressions, $n_p$ and $B_0$ are the density of the plasma protons and the magnitude of the initial magnetic field, respectively, while $e$ and $m_p$ are the

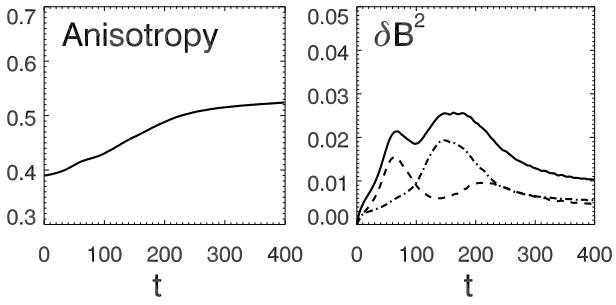


**Figure 2.** Simulation: Evolution of (lef) the temperature anisotropy $T_\perp/T_\parallel$ and (right) the total fluctuating magnetic energy $\delta B^2$ (solid curve). Dashed curves moreover show the fluctuating magnetic energy in waves with $\theta_{\boldsymbol{kB}} < 30^\circ$ (dashed curve) and $\theta_{\boldsymbol{kB}} > 30^\circ$ (dash-dotted curve).

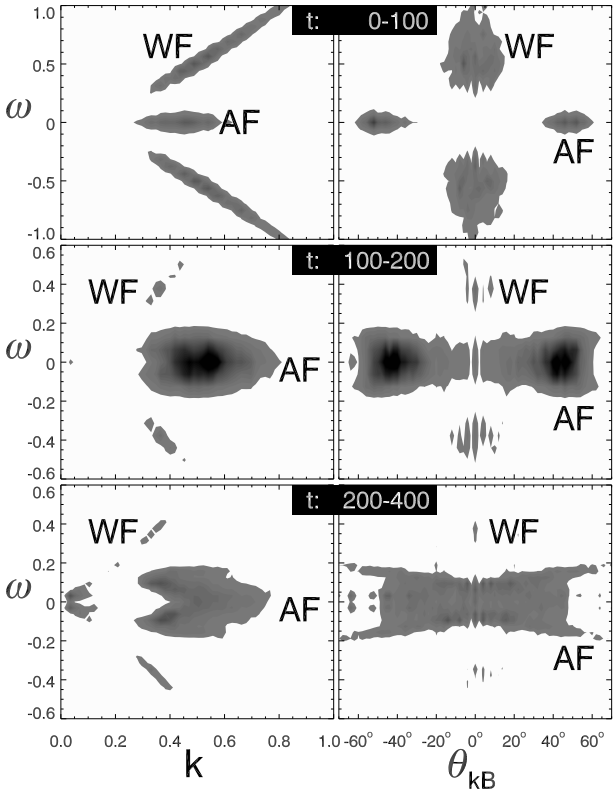


**Figure 3.** Simulation spectrum: (left) $\delta B$ as a function of $k$ and $\omega$ and (right) $\delta B$ as a function of $\theta_{\boldsymbol{kB}}$ and $\omega$. Simulations are shown for $t$=0–100, $t$=100–200, and $t$=200–400. All the left panels use the same gray scale, and another one is used for all the right panels. WF, whistler fire hose; AF, Alfvén fire hose.

proton electric charge and mass, respectively; finally, $c$, $\epsilon_0$, and $\mu_0$ are the speed of light and the dielectric permitivity and magnetic permeability of vacuum, respectively. The spatial resolution is $dx = dy = c/\omega_{pi}$, and there are 256 particles per cell. The simulation box is in the $xy$ plane and is assumed to be periodic in both dimensions. The fields and moments are defined on a 2-D grid with dimensions $n_x \times n_y = 256 \times 128$. The time step for the particle advance is $dt = 0.02\Omega_i^{-1}$ while the magnetic field $\boldsymbol{B}$ is advanced with a smaller time step, $dt_B = dt/10$. Velocities are given in units of $v_A$. The same units are used in Figures 2–4. The relevant plasma parameters are the ratio $T_{p\perp}/T_{p\parallel}$ and plasma betas, ratios between particle pressures and the magnetic pressure $p_B = B_0^2/(2\mu_0)$: The electron beta $\beta_e = n_p k_B T_e/p_B$, the proton parallel beta

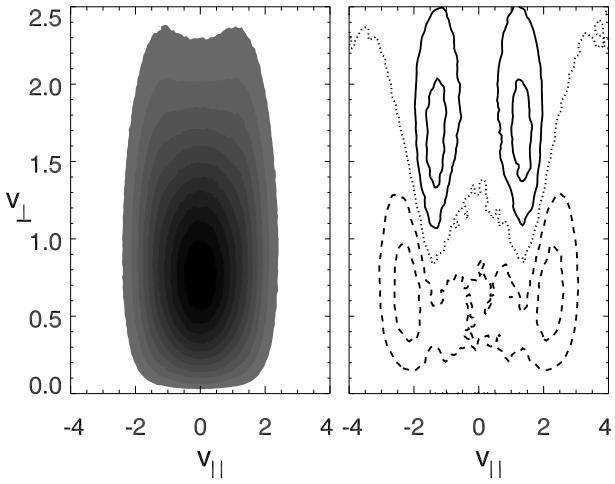


**Figure 4.** Simulation: (left) gray scale plot of the proton distribution function $f(v_\parallel, v_\perp)$ at the end of the simulation and (right) contour plot of $\Delta f = f(v_\parallel, v_\perp) - f_0(v_\parallel, v_\perp)$, where $f_0(v_\parallel, v_\perp)$ is the initial proton distribution function (solid curves denote $\Delta f > 0$, dashed curves denote $\Delta f < 0$, and dotted curve denotes $\Delta f = 0$).

$\beta_{p\parallel} = n_p k_B T_{p\parallel}/p_B$, where $k_B$ is Boltzmann constant, and $T_e$ is electron temperature. We initialize the simulation with homogeneous bi-Maxwellian protons with $\beta_{p\parallel} = 2.8$ and $T_{p\perp}/T_{p\parallel} = 0.4$ (compare paper 1) in an initially constant magnetic field $\boldsymbol{B}_0$ directed along the $x$ axis, $\boldsymbol{B}_0 = (B_0, 0, 0)$. For these plasma parameters the two instabilities are present, and the Alfvén fire hose has a slightly greater maximum growth rate ($\gamma_{AFm} = 0.059$) than does the whistler fire hose ($\gamma_{WFm} = 0.056$).

### 2.2. Results

Let us now describe the results of the 2-D simulation and compare it to the 1-D simulations of paper 1. Initially, both the instabilities generate waves for a wide range of wave vectors $k$ and propagation angles $\theta_{\boldsymbol{kB}}$ with respect to the magnetic field, in agreement with the prediction of linear theory. Figure 2 shows the evolution of the temperature anisotropy $T_\perp/T_\parallel$ (left panel) and the total fluctuating magnetic energy $\delta B^2$ (right panel) in the same format as that in Figure 1. Figure 2 (right panel) also shows the repartition of the fluctuating magnetic energy in waves with $\theta_{\boldsymbol{kB}} < 30^\circ$ (dashed curve) and $\theta_{\boldsymbol{kB}} > 30^\circ$ (dash-dotted curve). During the initial period $t \sim$ 0–100, the dashed curve shows the evolution of the whistler fire hose while the dash-dotted curve shows the evolution of the Alfvén fire hose. Figure 2 (right panel, dashed curve) demonstrates that the whistler fire hose grows first (the initial perturbations dominate at parallel propagation), saturates rapidly, and soon decays during the initial stage, while the Alfvén fire hose is still growing (Figure 2, right panel, dash-dotted curve). The saturation of the whistler fire hose is in a quasi-linear manner as we infer from the 1-D simulation (see Figure 1 and, for details, paper 1); the saturation level (for the two instabilities) is lower than that in one dimension (compare Figure 1) owing to the higher dimensionality effects (oblique waves driven by the whistler fire hose enhance the pitch angle scattering of protons [*Karimabadi et al.*, 1992; *Gary et al.*, 1998]) and, naturally, owing to the presence of the other instability. The fast decay of the waves driven by the whistler fire hose is also partly due to the dimensionality effects (see above) but mainly is due to the presence of the Alfvén fire hose. The Alfvén fire hose importantly heats the protons (compare left panels of Figures 1 and 2) and therefore disrupts the marginal stability condition for the whistler fire hose.

Later on, the Alfvén fire hose saturates, and the wave activity decays and shifts to the less oblique propagation angles $\theta_{\boldsymbol{kB}}$. Since

the evolution of temperature anisotropy in the 1-D Alfvén fire hose simulation and that in the present 2-D one are similar (compare left panels of Figures 1 and 2), we expect that the Alfvén fire hose converts to Alfvén waves (as observed in the 1-D simulation of paper 1). We also expect that the generated Alfvén waves damp to the protons and decay via a wave coupling to long-wavelength and less oblique waves giving a rise to an increase of the fluctuating magnetic energy in waves with $\theta_{\boldsymbol{kB}} < 30^{\circ}$ (Figure 2, right panel, dashed curve). Let us now verify our expectations.

Figure 3 shows the wave spectrum $\delta B$ as a function of $k$ and $\omega$ (left panels) and $\theta_{\boldsymbol{kB}}$ and $\omega$ (right panels), respectively, during the different time intervals (compare Figure 2): $t$=0–100, $t$=100–200, and $t$=200–400. Note that there are two gray scales used in Figure 3: one for all the left panels and another one for all the right panels. Figure 3 (top panels) demonstrates the coexistence of the two instabilities: the whistler fire hose at parallel propagation and the zero-frequency Alfvén fire hose at strongly oblique propagation.

Figure 3 (middle panels) shows that the Alfvén fire hose dominates the simulation at $t$=100–200 and that the whistler fire hose is strongly suppressed (see Figure 2). Figure 3 (bottom panels) demonstrates the same kind of evolution as that seen in the one-dimensional simulation (paper 1): The dominating, zero-frequency Alfvén fire hose converts to finite frequency Alfvén waves that are damped (via cyclotron resonance with protons as we check later) and decay via wave-wave coupling to long-wavelength and less oblique Alfvén waves. The two-dimensionality of the present simulation naturally allows a coupling between more waves, and therefore the final wave spectrum is wider and more important than that observed in the one-dimensional simulation of paper 1 (see Figures 1 and 2).

Finally, let us have a look at the impact of the wave-particle interactions on the proton distribution function. Figure 4 (left panel) shows the gray scale plot of the proton distribution function $f(v_{\parallel}, v_{\perp})$ at the end of the simulation. Figure 4 (right panel) displays the contour plot of $\Delta f = f(v_{\parallel}, v_{\perp}) - f_0(v_{\parallel}, v_{\perp})$, where $f_0(v_{\parallel}, v_{\perp})$ is the initial, bi-Maxwellian proton distribution function (solid curves denote $\Delta f > 0$, dashed curves denote $\Delta f < 0$, and dotted curve denotes $\Delta f = 0$). Figure 4 (left panel) indicates non bi-Maxwellian features: the "ears" around $v_{\perp} > 2$ and $|v_{\parallel}| \sim 1$. Figure 4 (right panel) clearly demonstrates that there is an excess (comparing to the initial distribution function) of protons with $|v_{\parallel}| \sim 1.5$ and $v_{\perp} \sim 1.5 - 2$ and that these particles come from the regions with $|v_{\parallel}| \sim 2$ and $v_{\perp} \sim 0.5 - 1$. This effect is compatible with an acceleration via the cyclotron resonance; a rough estimation gives a phase velocity $v_{ph}$ of resonant waves lower than $v_A$. Therefore the protons has mainly been accelerated via the cyclotron resonance with the Alfvén waves generated by the Alfvén fire hose (see Figure 3 and paper 1).

## 3. Conclusion and Discussion

We have studied the competition between the whistler and Alfvén fire hoses. We have performed a 2-D hybrid simulation for the following initial plasma parameters: $\beta_{p\parallel} = 2.8$ and $T_{p\perp}/T_{p\parallel} = 0.4$. The two instabilities have different properties as well as nonlinear evolutions: The whistler fire hose initially dominates (grows for a wide range of wave vectors) but rapidly saturates in a quasi-linear manner in agreement with *Gary et al.* [1998] and the 1-D simulation of paper 1. Meanwhile, the Alfvén fire hose grows and continues to grow even when the whistler fire hose is saturated. As the Alfvén fire hose heats the plasma protons, the marginal stability condition for the whistler fire hose is overcome, and the waves driven by the whistler fire hose are strongly damped. The later stage of the simulation is dominated by the Alfvén fire hose: The Alfvén fire hose saturates via a conversion to the Alfvén waves. The Alfvén waves are strongly damped, but a part of their energy cascades via wave-wave coupling to long-wavelength, less oblique Alfvén waves.

The results of the 2-D hybrid simulation are in good agreement with the 1-D simulations of paper 1. The main difference is, of course, due to the interaction between the two instabilities. The Alfvén fire hose during its nonlinear evolution suppresses the waves driven by whistler fire hose. Furthermore, the final cascade of Alfvén waves goes through a wider range of canals (thanks to two-dimensionality of the simulation), and so the amount of cascading energy is more important in 2-D simulation than it is in 1-D simulation (compare paper 1).

Let us now try to predict the behavior of anisotropic nearly bi-Maxwellian protons with $T_{p\parallel} > T_{p\perp}$ for medium betas (compare paper 1) combining results of *Gary et al.* [1998], paper 1, and this paper. The key parameter which determines the behavior of the system is $\Delta\beta = \beta_{p\parallel}(1 - T_{p\perp}/T_{p\parallel})$. For $\Delta\beta < 1.5$ the whistler fire hose dominates, and we expect the quasi-linear evolution [*Gary et al.*, 1998]. For $1.9 > \Delta\beta > 1.5$ the Alfvén fire hose has a stronger growth rate, and we expect behavior similar to that presented in the present paper. For $\Delta\beta > 1.9$ the Alfvén fire hose has a smaller growth rate then does the whistler fire hose. However, if the Alfvén fire hose acquires enough energy during the linear stage, the evolution of the system will be similarly affected by its presence. To check this expectation we have performed another 2-D hybrid simulation for $\beta_{p\parallel} = 2.8$ and $T_{p\perp}/T_{p\parallel} = 0.2$ ($\Delta\beta = 2.24$); in this case the Alfvén fire hose has a smaller maximum growth rate ($\gamma_{AFm} = 0.12$) than does the whistler fire hose ($\gamma_{WFm} = 0.14$), but we observe an evolution similar to that for the case of $\beta_{p\parallel} = 2.8$ and $T_{p\perp}/T_{p\parallel} = 0.4$ studied in detail in the present paper. Therefore the Alfvén fire hose is important also for $\Delta\beta > 1.9$. However, we expect that for some greater values of $\Delta\beta$ the whistler fire hose again dominates the physics; we expect that in this case of strong proton anisotropy the quasi-linear approximation is not valid.

Let us now briefly discuss a relevance of the marginal stability approach [*Manheimer and Boris*, 1977; *Gary et al.*, 1998] for a general anisotropic proton distribution with $T_{p\parallel} > T_{p\perp}$. The previous discussion suggests that the marginal stability approach works for bi-Maxwellian protons with a small anisotropy (small $\Delta\beta$) where the role of the Alfvén fire hose is negligible. If we assume that for small anisotropies the role of the Alfvén fire hose is marginal for all (reasonable) proton distribution functions, then the prediction of *Gary et al.* [1998] based on the marginal stability analysis would be significantly robust. However, in the present simulation we find an example of the previous assumption not being valid: During the initial phase, after the stabilization of the whistler fire hose, the Alfvén fire hose continues to be unstable. Therefore we conclude that the marginal stability approach [*Manheimer and Boris*, 1977; *Gary et al.*, 1998] is not generally valid for anisotropic proton distributions with $T_{p\parallel} > T_{p\perp}$ because of the existence of the Alfvén fire hose: The Alfvén fire hose has an atypical, non-quasi-linear evolution due to the transitory behavior of the unstable mode, disrupts the quasi-linear evolution of the whistler fire hose, and makes the waves driven by the whistler fire hose disappear. The simulation results also suggest that the relative importance of the two instabilities is very sensitive to the details of the distribution function [cf. *Gary*, 1991], since the whistler fire hose is generally a resonant instability [*Gary et al.*, 1998].

## References


Gary, S. P., Electromagnetic ion/ion instabilities and their consequences in space plasma: A review, *Space Sci. Rev.*, *56*, 373–414, 1991.

Gary, S. P., H. Li, S. O'Rourke, and D. Winske, Proton resonant firehose instability: Temperature anisotropy and fluctuating field constraints, *J. Geophys. Res.*, *103*, 14,567–14,574, 1998.

Hellinger, P., and A. Mangeney, Electromagnetic ion beam instabilities: Oblique pulsations, *J. Geophys. Res.*, *104*, 4669–4680, 1999.

Hellinger, P., and H. Matsumoto, New kinetic instability: Oblique Alfvén fire hose, *J. Geophys. Res.*, *105*, 10,519–10,526, 2000.

Karimabadi, H., D. Krauss-Varban, and T. Teresawa, Physics of pitch angle scattering and velocity diffusion, 1, Theory, *J. Geophys. Res.*, *97*, 13,853–13,864, 1992.

Manheimer, W., and J. P. Boris, Marginal stability analysis: A simpler approach to anomalous transport in plasmas, *Comments Plasma Phys. Controlled Fusion*, *3*, 15–24, 1977.

Matthews, A., Current advance method and cyclic leapfrog for 2D multispecies hybrid plasma simulations, *J. Comput. Phys.*, *112*, 102–116, 1994.

Quest, K. B., and V. D. Shapiro, Evolution of the fire-hose instability: Linear theory and wave-wave coupling, *J. Geophys. Res.*, *101*, 24,457–24,469, 1996.

P. Hellinger, Institute of Atmospheric Physics, Prague 141 31, Czech Republic. (helinger@ufa.cas.cz)

H. Matsumoto, Radio Science Center for Space & Atmosphere, Kyoto University, Uji 611-0011, Japan.
(matsumot@kurasc.kyoto-u.ac.jp)